4884 *Biochemistry* **2010,** *49,* 4884–4896
DOI: 10.1021/bi100097f

BIOCHEMISTRY
including biophysical chemistry & molecular biology
*Article*

# Rational Engineering of Mannosyl Binding in the Distal Glycone Subsites of *Cellulomonas fimi* Endo-$\beta$-1,4-mannanase: Mannosyl Binding Promoted at Subsite −2 and Demoted at Subsite −3[†,‡]

Omid Hekmat,[§] Leila Lo Leggio,[∥] Anna Rosengren,[§] Jurate Kamarauskaite,[∥,⊥] Katarina Kolenova,[§] and Henrik Stalbrand*[,§]

[§]*Department of Biochemistry, Center for Chemistry and Chemical Engineering, Lund University, Box 124, SE-221 00 Lund, Sweden,* [∥]*Biophysical Chemistry Group, Department of Chemistry, University of Copenhagen, Universitetsparken 5, DK-2100 Copenhagen, Denmark, and* [⊥]*Department of Biology, University of Copenhagen, Ole Maaløes Vej 5, DK-2200 Copenhagen, Denmark*

*Received January 21, 2010; Revised Manuscript Received April 28, 2010*

ABSTRACT: To date, rational redesign of glycosidase active-site clefts has been mainly limited to the removal of essential functionalities rather than their introduction. The glycoside hydrolase family 26 endo-$\beta$-1,4-mannanase from the soil bacterium *Cellulomonas fimi* depolymerizes various abundant plant mannans. On the basis of differences in the structures and hydrolytic action patterns of this wild-type (but recombinantly expressed) enzyme and a homologous mannanase from *Cellvibrio japonicus*, two nonconserved amino acid residues at two distal glycone-binding subsites of the *C. fimi* enzyme were substituted, Ala323Arg at subsite −2 and Phe325Ala at subsite −3, to achieve inverted mannosyl affinities in the respective subsites, mimicking the *Ce. japonicus* enzyme that has an Arg providing mannosyl interactions at subsite −2. The X-ray crystal structure of the *C. fimi* doubly substituted mannanase was determined to 2.35 Å resolution and shows that the introduced Arg323 is in a position suitable for hydrogen bonding to mannosyl at subsite −2. We report steady-state enzyme kinetics and hydrolysis-product analyses using anion-exchange chromatography and a novel rapid mass spectrometric profiling method of $^{18}$O-labeled products obtained using $H_2{}^{18}O$ as a solvent. The results obtained with oligosaccharide substrates show that although the catalytic efficiency ($k_{cat}/K_m$) is wild-type-like for the engineered enzyme, it has an altered hydrolytic action pattern that stems from promotion of substrate binding at subsite −2 (due to the introduced Arg323) and demotion of it at subsite −3 (to which removal of Phe325 contributed). However, $k_{cat}/K_m$ decreased ∼1 order of magnitude with polymeric substrates, possibly caused by spatial repositioning of the substrate at subsite −3 and beyond for the engineered enzyme.

Secondary plant cell walls are highly complex structures composed of lignin and an interlocking network of polysaccharides, mainly cellulose and hemicellulose. The major softwood hemicellulose is acetylated galactoglucomannan which is a heteropolymer with a $\beta$-1,4-linked backbone of D-mannopyranosyl and D-glucopyranosyl units bearing different degrees of α-1,6-D-galactopyranosyl and/or acetyl (O2 or O3) substitution (*1*, *2*). Endo-$\beta$-1,4-mannanases (EC 3.2.1.78) are glycoside hydrolases (GHs)[1] that belong to GH families 5, 26, and 113 (http://www.cazy.org/) (*3*) and catalyze the hydrolysis of $\beta$-1,4-mannosidic bonds in mannans and heteromannans (Scheme 1). GH families 5 and 26 belong to the 4/7 superfamily, clan GH-A, whose members share the $(\beta/\alpha)_8$ barrel fold (*4*, *5*) and a retaining double-displacement reaction mechanism (*6*). Endo-$\beta$-1,4-mannanases often have additional modules such as carbohydrate-binding modules (CBM) as well as a catalytic module (CD) (*7*, *8*).

Crystal structures of several GH5 (*9*−*12*) and GH26 $\beta$-mannanases (*13*−*19*) have been determined. Like many other glycanases, the CDs of mannanases usually have several glycone (negative numbering) and aglycone (positive numbering) sugar-binding subsites where the mannosidic bond between the adjacent monomers occupying subsites −1 and +1 is cleaved (*20*). Known $\beta$-mannanases and $\beta$-mannosidases are defined by a proximal glycone −1 subsite that is invariably specific for a mannose residue through a high level of structural conservation (*14*, *19*) (Figure 1). It appears that the topology of subsite −1 is tuned toward binding a mannose ring in its boatlike ($B_{2,5}$) conformation near or at the transition state (*14*, *19*, *21*). On the other hand, some GH5 and GH26 $\beta$-mannanases differ in terms of the

[†]This work was supported by grants to H.S. from the Swedish Research Council (VR) (40467101) and the Crafoord Foundation, as well as a grant to L.L.L. from the Carlsberg Foundation (2005-1-500). L.L.L. thanks DANSCATT (Danish National Research Council) and the European Community-Research Infrastructure Action under the FP6 for support of synchrotron access. O.H. was supported by postdoctoral fellowships from the Swedish Institute and the Sven and Lilly Lawskis Foundation.

[‡]The structure described in this article has been deposited with the Protein Data Bank as entry 2x2y.

*To whom correspondence should be addressed. Telephone: +46-46-2228202. Fax: +46-46-2224116. E-mail: henrik.stalbrand@biochemistry.lu.se.

[1]Abbreviations: CBM, carbohydrate-binding module; CD, catalytic module; CfMan26A, full-length modular wild-type endo-$\beta$-1,4-mannanase from *Cellulomonas fimi*; CjMan26A, nonmodular wild-type endo-$\beta$-1,4-mannanase from *Cellvibrio japonicus* (previously *Pseudomonas cellulosa*); DM, double mutation; DM-CfMan26A-50K, recombinant amino-terminal 50 kDa stable fragment of endo-$\beta$-1,4-mannanase from *C. fimi* with the A323R and F325A substitutions created by a double mutation; DNS, 3,5-dinitrosalicylic acid; GG, guar gum galactomannan; GH, glycoside hydrolase; HPAEC-PAD, high-performance anion-exchange chromatography with pulsed amperometric detection; Ig, immunoglobulin; LBG, locust bean gum galactomannan; MALDI-TOF MS, matrix-assisted laser desorption ionization time-of-flight mass spectrometry; $M_n$, $\beta$-1,4-linked manno-oligosaccharide of *n* degrees of polymerization; NCS, noncrystallographic symmetry; PCR, polymerase chain reaction; PDB, Protein Data Bank; rmsd, root-mean-square deviation; SLH, S-layer homology; TLC, thin-layer chromatography; WT, wild-type; WT-CfMan26A-50K, recombinant amino-terminal 50 kDa stable fragment of wild-type endo-$\beta$-1,4-mannanase from *C. fimi*.

 Published on Web 04/28/2010 

Scheme 1: Endo-$\beta$-1,4-mannanase-Catalyzed Hydrolysis of a Manno-Oligosaccharide $M_{(x+y)}$ to Smaller Manno-Oligosaccharide products $M_x$ and $M_y$[a]

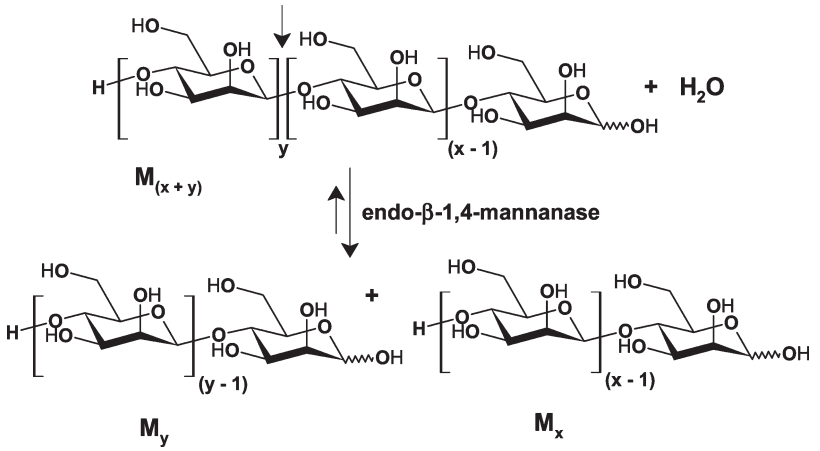


[a]The arrow points to the mannosidic bond to be cleaved.

tightness of mannose specificity of subsites flanking the critical −1 subsite (*19*).

The endo-$\beta$-1,4-mannanase from *Cellulomonas fimi* (CfMan26A) is comprised of five modules (*16*, *22*), including an internal mannan-binding CBM of family 23 (*23*). The crystal structure of a 50 kDa recombinant truncated enzyme variant (WT-CfMan26A-50K) with wild-type (WT) sequence but comprising only the N-terminal GH26 CD and the immunoglobulin-like (Ig-like) module was previously determined (*16*). Here, we report on the analysis of a variant (DM-CfMan26A-50K) of this protein with two substituted residues created by a double mutation (DM). The rationale behind the engineering of the glycone-binding distal subsites of WT-CfMan26A-50K came from the comparison of the structure and the hydrolytic action pattern of WT-CfMan26A-50K (*16*) to those of another well-characterized and homologous GH26 endo-$\beta$-mannanase, CjMan26A from *Cellvibrio japonicus* (*13*−*15*). The catalytic domain of WT-CfMan26A-50K is 34% identical in sequence to CjMan26A, and their structures have several common features. This is shown by overlay analysis in which the structures of WT-CfMan26A-50K in complex with mannotriose bound at subsites −2 to −4 (PDB entry 2bvt) and the CjMan26A-Glu320Gly variant in a complex with mannobiose bound at subsites −1 and −2 (PDB entry 1odz) superimpose with a 1.1 Å rmsd based on 339 $C_\alpha$ atoms. No major structural differences are observed in the vicinity of subsites +1 and −1, with key conserved residues involved in substrate binding and catalysis (*13*, *16*, *19*, *24*, *25*) (Figure 1). Glu175 and Glu282 in WT-CfMan26A-50K (Glu212 and Glu320 in CjMan26A, respectively) are the catalytic acid/base and nucleophile residues, respectively.

In contrast, structural differences are observed between the two enzymes at subsites −2 and −3 (*13*, *15*, *16*), with non-conserved amino acids as candidates responsible for the differences in the hydrolytic patterns of these two enzymes. Two amino acids at subsite −2 are in equivalent positions in both enzymes and interact with the mannosyl in subsite −2 by hydrogen bonds or polar contacts (Glu78 and Gln329 in WT-CfMan26A-50K and Glu121 and His377 in CjMan26A). However, a striking difference is that Arg361 of CjMan26A forms hydrogen bonds to the C2 and C3 hydroxyls of the mannosyl in subsite −2, but these interactions are lacking in WT-CfMan26A-50K since the equivalent residue is Ala323 (Figure 1) (*16*). In a recent study, Tailford et al. showed that Arg361 in CjMan26A and an equivalent residue (Arg374) in an exomannanase, CjMan26C, confer high mannose (vs glucose) specificity by interacting with the axial C2 hydroxyl of the $^4C_1$ ground-state mannose unit (*17*, *19*). Conversely, Phe325 at subsite −3 of WT-CfMan26A-50K provides a hydrophobic stacking platform for the mannose unit (*16*), but this interaction is missing in CjMan26A since the equivalent residue is Ala363 (Figure 1). The structural data alone thus may indicate that the relative affinities at subsites −2 and −3 are inverted in the two enzymes.

The differences in the hydrolytic action patterns of these two enzymes are most pronounced for mannotetraose ($M_4$) hydrolysis. Previous work showed that $M_4$ forms a major productive complex with WT-CfMan26A-50K, binding from the −3 to +1 subsites, thus forming $M_3$ and $M_1$ as major products (*16*, *24*). For CjMan26A, $M_4$ is preferentially productively bound from the −2 to +2 subsites since $M_2$ is the major hydrolysis product (*13*). Thus, these observations are consistent with the inverted affinities within subsites −3 and −2 hypothesized above. Furthermore, Tailford et al. recently showed the importance of Arg361 in subsite −2 of CjMan26A: an Ala substitution decreased the observed $k_{cat}/K_m$ dramatically (2750 times for $M_4$) (*19*). To gain further insights into the engineering of substrate-binding residues among GH26 enzymes, we report here on the creation and analysis of a doubly substituted variant of the *C. fimi* $\beta$-mannanase (DM-Man26A-50K). In this work, we set out to determine the structural and functional consequences of redesigning the distal glycone-binding subsites of WT-CfMan26A-50K through the removal of the important Phe325 at subsite −3, leaving space for the introduction of a "high-affinity Arg323" [term coined by Tailford et al. (*19*)] at subsite −2, positioned like Arg361 in CjMan26A. The Ala323Arg/Phe325Ala enzyme variant was analyzed via structural and biochemical methods.

## EXPERIMENTAL PROCEDURES

*General Materials and Methods*. Manno-oligosaccharides (mannobiose $M_2$, mannotriose $M_3$, mannotetraose $M_4$, mannopentaose $M_5$, and mannohexaose $M_6$) were purchased from Megazyme (Bray, Ireland). Isotopically labeled $H_2{}^{18}O$ (normalized 97 atom %) was from Isotec, Aldrich (Steinheim, Germany); restriction enzymes were from Fermentas (St. Leon-Rot, Germany) and synthetic oligonucleotides from TAGC

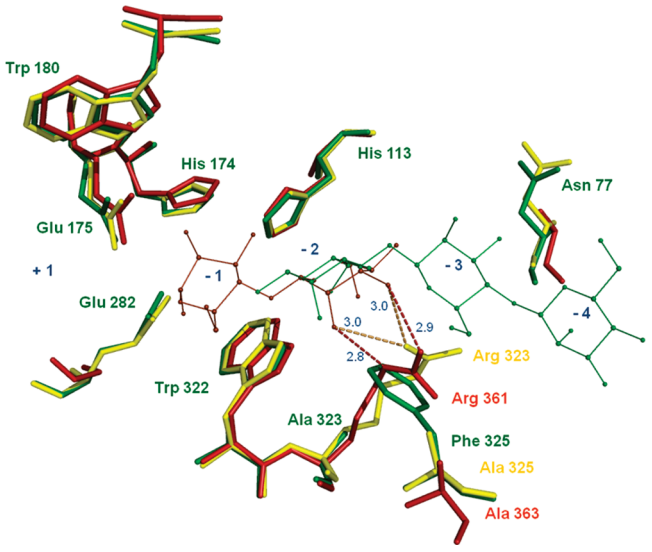


FIGURE 1: Superposition of substrate binding grooves of WT-CfMan26A-50K in complex with $M_3$ in subsites −4 to −2 (PDB entry 2bvt) (green), DM-CfMan26A-50K (yellow), and CjMan26A-Glu320Gly in a complex with $M_2$ at subsites −2 and −1 (PDB entry 1odz) (red). Gln329 in WT- and DM-CfMan26A-50K (His377 in CjMan26A), involved in axial O2 specific recognition, is not shown for the sake of clarity. Putative hydrogen bonds between Arg323 and Arg361 at subsite −2 and the C2 and C3 hydroxyls of $M_2$ from the CjMan26A complex are shown. The figure was made with Pymol (The PyMOL molecular graphics system, DeLano Scientific LLC, San Carlos, CA).

(Copenhagen, Denmark). All other chemicals were obtained in reagent grade from Sigma/Aldrich Chemical Co. (Schnelldorf, Germany). Protein concentrations were determined using the Micro BCA Protein Assay Reagent Kit with BSA standards (Pierce, Rockford, IL).

*Site-Directed Mutagenesis*. Mutagenesis was performed using the overlap extension technique (*26*). First, the DM-CfMan26A-50K gene was amplified in two parts in two separate PCRs each using plasmid pET28b/WT-Man26A-50K (*16*) as a template and either primer pair fwd1 and rev1 (5′-TGCTCG-AGTGCGGCC-3′ and 5′-CGTGGAGGAATGCCGACGCC-GGCCAG-3′, respectively) or primer pair fwd2 and rev2 (5′-CG-TCGGCATTCCTCCACGTCTCCATGTAGG-3′ and 5′-GG-CGACTTTCCCGCG-3′, respectively). Primers rev1 and fwd2 are both complementary to the site of mutagenesis but include six noncomplementary base pairs (mismatches, underlined) creating the A323R and F325A mutations. fwd1 includes a NotI (underlined) and rev2 a SacII (Cfr42I) (underlined) restriction site. The products of these two PCRs were purified on an agarose gel and used together as templates in a second PCR using primers fwd1 and rev2 to amplify the whole gene. The final PCR product was purified on an agarose gel and rescued with rescue vector pCR-Blunt II-TOPO (Invitrogen Life Sciences, Carlsbad, CA) using the Zero Blunt TOPO PCR cloning protocol from Invitrogen. Plasmid pCR-BluntII-TOPO/DM-CfMan26A-50K was double-restriction-digested using NotI and SacII, and the DM-CfMan26A-50K gene (harboring the A323R and F325A mutations) was inserted into the similarly double-restriction-digested pET28b/WT-Man26A-50K plasmid and sequenced.

*Protein Expression and Purification*. Recombinant WT-CfMan26A-50K (475 amino acids, 50416 Da; amino acids 1−464 of mature modular WT-CfMan26A and an added C-terminal AAALEHHHHHH sequence) and recombinant DM-CfMan26A-50K (475 amino acids, 50426 Da; exactly the same as the WT construct except for the substituted residues) were expressed by *Escherichia coli* cells and purified as described previously (*16*) with minor changes. Briefly, BL21(DE3) cells were transformed (electroporation) with plasmid pET28b (Novagen, Madison, WI) harboring either the WT or DM insert. Cell lysis (French press) was performed in QIAGEN NPI-10 binding/lysis buffer [50 mM sodium phosphate, 300 mM NaCl, and 10 mM imidazole (pH 8.0)]. Cleared cell lysate was loaded onto a 1 mL Ni-NTA Superflow cartridge (QIAGEN), and the His-tagged protein was eluted with a linear gradient from 10 to 130 mM imidazole [50 mM sodium phosphate and 300 mM NaCl (pH 8.0)] at a flow rate of 1.0 mL/min over 80 min. Fractions (2.5 mL) were analyzed via SDS−PAGE (6 cm, 4 to 12% gradient gel, Invitrogen) and assayed for $\beta$-1,4-mannanase activity using reducing-sugar detection with 2-hydroxy-3,5-dinitrobenzoic acid (DNS) (*27*). After three rounds of Ni-ion-affinity chromatography, both WT- and DM-CfMan26A-50K appeared as single bands (50 kDa) when analyzed via SDS−PAGE (Coomassie staining) using a 6 cm, 4 to 12% gradient gel.

*Crystallization*. Crystallization trials were conducted in a 96-well MRC plate (three-protein well version) with a 50 $\mu$L reservoir and 0.3 $\mu$L drops containing varying proportions of reservoir and protein solution at a concentration of 8.4 mg/mL in 50 mM sodium citrate buffer (pH 6.0). The drops were dispensed using an Oryx 8 protein crystallization robot (Douglas Instruments). X-ray quality crystals were obtained with condition 5 in the JCSG+ crystallization suite (QIAGEN), having 0.2 M magnesium formate (pH 5.9) and 20% PEG 3350 in the reservoir.

*Data Collection and Processing*. Glycerol was added to the mother liquor to a final concentration of 20% (v/v) as a cryoprotectant. A crystal of DM-CfMan26A-50K was flash-cooled in liquid nitrogen, and data were collected at 100 K after the mixture had been annealed once in situ to reduce the high mosaicity. Data collection was accomplished on beamline 911-2 at MAXLAB (Lund, Sweden), with a crystal-to-detector distance of 150 mm, an oscillation range of 0.5° per frame, and a wavelength of 1.0379 Å. Data were processed with MOSFLM version 7.0.1 (*28*) and SCALA version 3.2.5 (*29*) in the CCP4 package. The space group was $P2_12_12_1$ with two molecules in the asymmetric unit and the following unit cell dimensions: $a$ = 73.1 Å, $b$ = 99.6 Å, and $c$ = 133.0 Å. Data processing statistics are listed in Table 1.

*Structure Determination and Refinement*. The structure of DM-CfMan26A-50K was determined by molecular replacement with MOLREP (*32*) using the uncomplexed WT-CfMan26A-50K [PDB entry 2bvy (*16*)] as a model. The crystal of DM-CfMan26A-50K was in fact essentially isomorphous to the mannotriose complex of WT-CfMan26A-50K [PDB entry 2bvt (*16*)], but since the uncomplexed WT structure had been determined at a significantly higher resolution, it was used as a model. A clear solution was identified with a correlation coefficient of 69.2% and an $R$-factor of 38.3%. The search results revealed noncrystallographic symmetry (NCS) where the two molecules in the asymmetric unit are related essentially only by translation. NCS restraints were applied between the two molecules in the asymmetric units in subsequent refinement steps. Five percent of the observed reflections were randomly removed for cross-validation, and the refinement was performed using maximum-likelihood program Refmac version 5.2.0005 (*33*). Toward the end of the refinement, the restraints for nine side chains were loosened as there were genuine differences for these residues in the electron density maps of the two molecules. Visual inspection

Table 1: Crystallographic Statistics[a]

| | |
|---|---|
| **Data Processing** | |
| no. of measured reflections | 245300 |
| no. of unique reflections | 41120 |
| resolution range (Å) | 19.43−2.35 (2.48−2.35) |
| multiplicity | 6.0 (5.6) |
| completeness (%) | 99.8 (99.9) |
| $R_{(r.i.m.)}$[b] (%) | 11.2 (38.1) |
| $I/\sigma(I)$ | 6.6 (2.1) |
| **Refinement** | |
| $R_{work}/R_{free}$ | 0.159/0.199 |
| root-mean-square deviation | |
| bond lengths (Å) | 0.009 |
| bond angles (deg) | 1.096 |
| Ramachandran plot (%)[c] | |
| most favored | 92.7 |
| additional allowed | 7.2 |
| generously allowed | 0.1 |
| disallowed | 0.0 |
| no. of non-H atoms | |
| protein | 6787 |
| water | 628 |
| Mg | 4 |
| formate | 24 |

[a]Statistics in parentheses refer to the outer resolution shell. [b]Redundancy-independent $R_{merge}$ (*30*): $R_{(r.i.m.)} = \sum_{hkl}[N/(N-1)]^{1/2}\sum_i I_i(hkl) - I_i(hkl)/\sum_{hkl}\sum_i I_i(hkl)$. [c]Calculated using PROCHECK (*31*).

and manual correction of the resulting model structures were accomplished using Coot (*34*) and alternated with the refinement. The final model comprises residues 4−465, with the additional following residues missing: 387−389 (missing only in molecule A), 412, 413, 436−442, 443, and 444 (missing only in molecule B). Some residual density that might belong to additional residues was observed at the termini and near chain breaks, but additional amino acids were difficult to model because of the disorder and limited resolution. Two proline cis-peptides per molecule are found in the model (Pro80 and Pro380). Thirteen side chains (Asp12A/B, Glu30A/B, Arg79A/B, Glu84B, Arg232B, Glu341A, Gln373A, Gln403A, and Asp420A/B) were modeled with two alternate conformations. The rmsd for all atoms between the two chains, calculated using the lsq option in Coot, is 0.28 Å. The automated refinement procedure ARP/wARP (*35*) was applied for modeling solvent molecules, which were further checked visually. A total of 628 water molecules are included in the final model. Refinement resulted in identification of further components in the solvent area. Four strong electron density peaks were interpreted as $Mg^{2+}$ ions, two per protein molecule in the asymmetric unit, and binding at analogous sites in each molecule. In each molecule, one $Mg^{2+}$ ion is hexacoordinated by water molecules only, with typical coordination distances (between 2.00 and 2.23 Å). The second $Mg^{2+}$ ion is pentacoordinated by Thr352 (side chain and carbonyl oxygen) and the main chain oxygens of Ala347 and Asp349 as well as a water molecule, with coordination distances somewhat longer than usual (between 2.16 and 2.53 Å). Although erroneously interpreted as water, an ion, probably sodium, is also present in the original native structure at this site. We view the $Mg^{2+}$ ion binding as opportunistic binding because of the presence of 0.2 M $Mg^{2+}$ ions in the crystallization mixture. Eight formate ions, also originating from the crystallization mixture, were identified in the model. For each molecule in the asymmetric unit, two formate ions bind equivalently to the substrate binding groove. As cacodylate did in the WT-CfMan26A-50K structure, formate partly occludes subsite −1 and, additionally, subsite −2. The formate ion at subsite −1 makes hydrogen bonds to the catalytic nucleophile Glu282, as well as His174 and His113, while the formate ion at subsite −2 makes hydrogen bonds to Glu78 and one or two water molecules. An additional formate ion is bound at the B molecule substrate-binding groove through a water-mediated hydrogen bond. Three additional formate ions bind away from the substrate binding groove, giving a total of eight formate ions in the structure. The final model was refined to an *R* factor of 15.9% and an $R_{free}$ of 19.9%. The refinement details are summarized in Table 1.

*Analysis of the Initial and End Products of Hydrolysis.* (*i*) *Initial Products*. Analysis of the initial hydrolysis products of manno-oligosaccharide substrates ($M_3$−$M_6$) catalyzed by WT-CfMan26A-50K has been reported previously (*16*). We repeated the analysis of the initial hydrolysis products of $M_4$ catalyzed by WT-CfMan26A-50K and conducted full analyses of the initial hydrolysis products of $M_3$−$M_6$ substrates catalyzed by DM-CfMan26A-50K under the same conditions that were used for WT-CfMan26A. For each substrate, the assay conditions and incubation times appropriate for the formation and observation of only the initial hydrolysis products were determined by analyzing test reactions by thin-layer chromatography (TLC). TLC was performed on aluminum-backed sheets of silica gel 60 $F_{254}$ plates (Merck) using a 10:8:7 (v/v/v) *n*-butanol/ethanol/water mixture as the eluent. Spots were visualized by exposure to a solution of *N*-(1-naphthyl)ethylenediamine dihydrochloride and sulfuric acid (*36*) followed by heating at 105 °C. Quantitative analysis of the formed initial hydrolysis products was achieved using high-performance anion-exchange chromatography with pulsed amperometric detection (HPAEC-PAD) as described previously (*7*, *16*). A DIONEX CX 500 system (Dionex, Sunnyvale, CA) equipped with an ED40 electrochemical detector and Carbo Pac PA-100 pre- and analytical columns were used. Solutions of appropriate standard manno-oligosaccharde mixtures at three different concentrations were also run on the DIONEX system along with samples from hydrolysis assays to set up standard plots (response vs concentration) for quantification. Elution was performed with 100 mM NaOH (for $M_3$, $M_5$, and $M_6$ hydrolysis assays) or 36 mM NaOH (for $M_4$ hydrolysis assays). Hydrolysis assays were performed at 37 °C in 50 mM sodium citrate buffer (pH 6.0) via incubation of 3.00 mM $M_4$ and 0.36 μg/mL WT-CfMan26A-50K for 30 min, 10.0 mM $M_3$ and 4.0 μg/mL DM-CfMan26A-50K for 30 min, 3.00 mM $M_4$ and 0.36 μg/mL DM-CfMan26A-50K for 90 min, or 3.00 mM $M_5$ or $M_6$ and 2.3 μg/mL DM-CfMan26A-50K for 22 min. The reactions were terminated when the mixtures were boiled.

(*ii*) *End Products*. For end-hydrolysis-product analysis, 3.33 g/L locust bean gum galactomannan (LBG) or $M_3$−$M_6$ substrates at the concentrations and assay conditions mentioned above were incubated with either 80 μg/mL WT-CfMan26A-50K or 0.40 mg/mL DM-CfMan26A-50K until complete hydrolysis was reached. Samples were run on the DIONEX system with 100 mM NaOH as the eluent.

*Steady-State Initial Velocity Kinetic Analysis*. All kinetic experiments were performed at 37 °C in 50 mM sodium citrate buffer (pH 6.0).

(*i*) *LBG and GG Substrates*. Steady-state kinetics of the WT- and DM-CfMan26A-50K-catalyzed hydrolysis of the polymeric substrates, LBG, and guar gum galactomannan (GG) were determined at 37 °C using a DNS stopped assay that detects

reducing sugars (*16*, *27*). The substrate and enzyme concentrations were as follows: 0.30−4.50 g/L LBG and either 0.33 μg/mL WT-CfMan26A-50K or 3.2 μg/mL DM-CfMan26A-50K and 0.56−18 g/L GG and either 0.33 μg/mL WT-CfMan26A-50K or 3.2 μg/mL DM-CfMan26A-50K. At each substrate concentration, a 400 μL aliquot of the assay was added to 600 μL of DNS at 5, 10, and 20 min time intervals. The absorbance at 540 nm was measured, and the amount of reducing sugar released was determined using a D-mannose standard curve. For each assay at a given substrate concentration, the reducing sugar concentration was plotted versus time and the initial velocity of hydrolysis was determined from a linear regression of the data with GraphPad Prism 4 (GraphPad Software, San Diego, CA). When no saturation was observed at practical substrate concentrations and the initial velocity curve ($V_o$ vs [S]) was linear, the value of $V_{max}/K_m$ was determined by linear regression. When the initial velocity curve was hyperbolic, the values of $K_m$ and $V_{max}$ were determined by fitting the data to the standard Michaelis−Menten equation using nonlinear regression with the same program.

(*ii*) *$M_3$−$M_6$ Substrates*. Steady-state kinetic parameters of the WT-CfMan26A-50K-catalyzed hydrolysis of oligomeric substrates $M_3$−$M_6$ have been reported (*16*). The steady-state kinetics of the DM-CfMan26A-50K-catalyzed hydrolysis of oligomeric substrates $M_3$−$M_6$ were also determined under the same conditions that were used for the WT enzyme using a stopped-assay method involving HPAEC with the DIONEX system as mentioned above. Elution was performed with 100 mM NaOH (for $M_3$ kinetics), 36 mM NaOH (for $M_4$ kinetics), or 48 mM NaOH (for $M_5$ and $M_6$ kinetics) as the eluent. Assay conditions were as mentioned above with 0.50−7.00 mM $M_3$ and 4.0 μg/mL DM-CfMan26A-50K, 0.50−4.00 mM $M_4$ and 0.36 μg/mL DM-CfMan26A-50K, 0.50−5.00 mM $M_5$ and 0.36 μg/mL DM-CfMan26A-50K, or 0.50−7.00 mM $M_6$ and 0.36 μg/mL DM-CfMan26A-50K. Aliquots were withdrawn at three time points during the 20−150 min incubation time, and the reactions were terminated when the mixtures were boiled. The formed hydrolysis products were then quantitatively analyzed on the DIONEX system. The total number of moles of the formed hydrolysis products at each time point was recalculated to the remaining number of moles of the substrate. The initial velocity curves ($V_o$ vs [S]) were hyperbolic, and the values of $K_m$ and $V_{max}$ were determined by fitting the data to the standard Michaelis−Menten equation using nonlinear regression with GraphPad Prism 4.

*Initial Hydrolysis of Manno-Oligosaccharide $M_3$−$M_6$ Substrates in $H_2{}^{18}O$ (solvent isotope incorporation)*. To determine and compare the WT- and DM-CfMan26A-50K-catalyzed hydrolytic cleavage patterns of $M_3$−$M_6$ substrates, initial hydrolysis assays were performed in $H_2{}^{18}O$ [with a total of 7% $H_2{}^{16}O$ contamination (3% in the original $H_2{}^{18}O$ and 4% from the enzyme and substrate stock solutions)]. In control experiments, $M_3$−$M_6$ were incubated in $H_2{}^{18}O$ under the assay conditions but without the enzyme at 37 °C and lower temperatures to assess the rate of nonenzymatic incorporation of $^{18}O$ at the anomeric center (C1) of the reducing end of manno-oligosaccharides. These experiments showed no detectable nonenzymatic $^{18}O$ incorporation at 8 °C but significant incorporation at higher temperatures (e.g., 22 and 37 °C) over the time period required for enzymatic hydrolysis (data not shown). Therefore, all enzymatic initial hydrolysis assays were performed at 8 °C in $H_2{}^{18}O$ (93%) containing 1 mM sodium citrate (pH 6.0), 0.8 mM $M_3$−$M_6$, and either 6.6 μg/mL[1] WT-CfMan26A-50K (32 μg/mL WT-CfMan26A-50K for $M_3$ hydrolysis) or 32 μg/mL DM-CfMan26A-50K. Aliquots of the hydrolysis samples were directly analyzed by MALDI-TOF MS as described below.

*MALDI-TOF MS*. Samples (0.5 μL) from hydrolysis assays were spotted directly onto a stainless steel MALDI target. A matrix solution containing 10 mg/mL 2,5-dihydroxybenzoic acid (gentisic acid) in water and acetonitrile (1:1) was added (0.5 μL) and dried using heated air. Control experiments showed that the short time (less than 1 min) required for the mixing of hydrolysis samples in $H_2{}^{18}O$ with the matrix solution in $H_2{}^{16}O$ and drying on a MALDI target did not cause any significant nonenzymatic $^{16}O$ back-incorporation at the anomeric center of $^{18}O$-labeled manno-oligosaccharides. MALDI-TOF mass spectra were recorded using a 4700 Proteomics Analyzer (Applied Biosystems, Framingham, MA) in positive reflector mode. The laser intensity was set between 6000 and 6400, and 70 subspectra, with 30 shots on each, were accumulated.

*MALDI-TOF MS Data Analysis*. For each substrate oligosaccharide, the relative frequencies (dominance) of the two productive binding modes of the substrate that gave rise to two same-DP products were deduced from the relative areas of a pair of light (no $^{18}O$ incorporation) and heavy ($^{18}O$-labeled at the anomeric center of the newly generated reducing end) monoisotopic MS peaks corresponding to one of the products. For example, for $M_4$, two different productive binding modes both gave rise to $M_3$ and $M_1$ products. The relative frequencies of these two modes were calculated from the relative areas of the monoisotopic MS peaks of $^{16}O$- and $^{18}O$-labeled $M_3$ products after two corrections: one for the [M + 2] natural isotope peak (5.3% of the monoisotopic peak for $M_3$) of the light ($^{16}O$) species that overlaps with the heavy ($^{18}O$) peak, followed by another correction for the 7% $H_2{}^{16}O$ contamination in the hydrolysis assays. The data were analyzed using Data Explorer version 4.6. $M_1$ was not detectable because of matrix suppression of low masses.

## RESULTS AND DISCUSSION

*Mutagenesis, Expression, and Basic Characterization*. The Ala323Arg/Phe325Ala doubly substituted variant of WT-CfMan26A-50K (DM-CfMan26A-50K), designed to mimic CjMan26A within subsites −2 and −3, was created by overlap extension PCR, expressed, and purified in the same manner as the WT enzyme. The pH dependence of the activity and temperature stability of both WT and DM enzymes were determined to be very similar (data not shown). Both are fully stable over 14 h at temperatures up to 30 °C and have optimal activity (> 90% of maximum) over a pH range of 5.5−7.0.

*Structure of DM-CfMan26A-50K*. DM-CfMan26A-50K was crystallized, and the three-dimensional (3D) structure was determined to be essentially the same as that of WT-CfMan26A-50K except around the two substitutions. It consists of an N-terminal $(\beta/\alpha)_8$ barrel (CD), typical of Clan GH-A enzymes, connected via a linker to a C-terminal Ig-like module of unknown function, which packs closely with the catalytic domain. The rmsd values for all atoms between WT-CfMan26A-50K and DM-CfMan26A-50K structures were 0.61 Å for chain A and 0.60 Å for chain B (0.30 and 0.29 Å, respectively, for $C_\alpha$ atoms only). If the catalytic domain and Ig-like domain are fit independently, rmsd values are 0.20 and 0.31 Å, respectively, for $C_\alpha$ atoms of chain A and 0.20 and 0.33 Å, respectively, for $C_\alpha$ atoms of chain B. Thus, there is no evidence of the relative movement of the two domains with respect to each other. The structure of

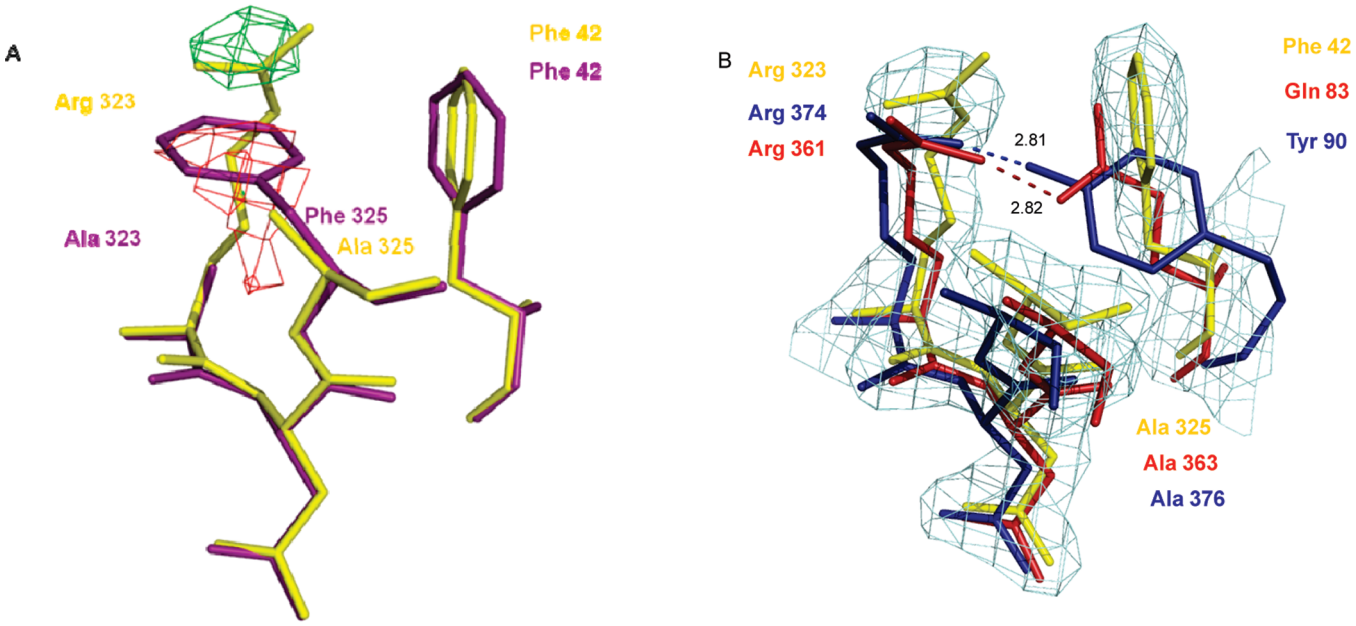


FIGURE 2: Electron density near the mutation site. (A) Initial difference map contoured at 3$\sigma$ (green) and −3$\sigma$ (red) calculated using phases from WT-CfMan26A-50K (purple). Clear negative density is visible on the substituted Phe325, while positive density is visible where Arg323 should be modeled. The final DM-CfMan26A-50K model is colored yellow for the sake of comparison. (B) View similar to that in panel A showing the final $2F_o - F_c$ map for DM-CfMan26A-50K contoured at 1$\sigma$. The DM-CfMan26A-50K model is colored yellow. Equivalent residues in the CjMan26A-Glu320Gly complex (PDB entry 1odz) and the CjMan26C complex (PDB entry 2vx7) are colored red and blue, respectively. Gln83 (CjMan26A) and Tyr90 (CjMan26C) can form hydrogen bonds with the Arg at subsite −2, while Phe42 (DM-CfMan26A-50K) cannot.

DM-CfMan26A-50K is also very similar to the reported structure of WT-CfMan26A-50K in a complex with $M_3$ bound at subsites −2 to −4 (*16*).

WT-CfMan26A-50K and CjMan26A share many residues interacting with substrate, as illustrated in Figure 1. One of the most significant differences is the one that the double mutation presented here seeks to emulate. Evidence of the amino acid substitutions was clear in the initial electron density maps for DM-CfMan26A-50K, and the introduced Arg323 at subsite −2 is very well-defined in the electron density for the final model (Figure 2). This is reflected in the average *B* factor of 19.4 Å$^2$ for Arg323 as compared to an average of 19.1 Å$^2$ for the whole protein chain. In the native uncomplexed structures available for CjMan26A (PDB entries 1j9y for the originally published structure and 1r7o for a later deposition, both to 1.85 Å resolution), the loop containing Arg361 at subsite −2 is poorly defined (*13*). Arg361 is not included in the model in 1j9y, and it is the last included residue for the loop in 1r7o, where it has a high *B* factor and is displaced from its position in complex structures. The orientation of the introduced Arg323 in the structure of DM-CfMan26A-50K is not the same as the equivalent Arg361 in the structure of CjMan26A-Glu320Gly in a complex with $M_2$ bound at subsites −1 and −2 (Figures 1 and 2) (*15*). While this could be ascribed to the fact that no oligosaccharides are bound in the DM-CfMan26A-50K structure, other factors must also be considered. CjMan26C in the same family also has Arg374 at the position equivalent to Arg323 in DM-CfMan26A-50K and Arg361 in CjMan26A (Figure 2) (*17*, *19*). Importantly, the orientation of Arg374 in either the uncomplexed structure of CjMan26C (PDB entry 2vx4) or the structure of CjMan26C in a complex with $M_2$ bound at subsites −1 and −2 (PDB entry 2vx7) is very similar to that of Arg361 in the structure of the CjMan26A-Glu320Gly−$M_2$ complex. It must be noted, however, that the apo structure of CjMan26C does have glycerol bound at the active site. In both CjMan26A and CjMan26C, the Arg side chain forms hydrogen bonds with a polar group (Gln83 in CjMan26A and Tyr90 in CjMan26C) through its NH1 group, whereas Arg323 in DM-CfMan26A-50K lacks such hydrogen bonding because the equivalent residue is Phe42 and has a conformation different from that of Tyr90 (Figure 2). Furthermore, in CjMan26C, Arg374 makes a salt bridge with Glu381. These factors may explain the different orientation of Arg323 in the uncomplexed DM enzyme, and it seems plausible that Arg323 would have the same orientation when a manno-oligosaccharide is bound. In any case, Arg323 is suitably positioned to interact with a mannosyl at subsite −2 as described below. So far, it has not been possible to determine a structure of the DM enzyme in complex with $M_2$ or $M_3$.

After superposition of the two structures, Arg323 in DM-CfMan26A-50K is too distant to interact with the mannosyl unit at subsite −2 of the WT-CfMan26A-50K/$M_3$ complex and clashes with the mannosyl unit at subsite −3 (1.9 Å between Arg NH2 and sugar C5 groups) (Figure 1). It is, however, more relevant to examine plausible interactions between Arg323 and the mannosyl unit at subsite −2 of the CjMan26A-Glu320Gly−$M_2$ complex since CjMan26A was the enzyme used as a template for redesigning subsites −2 and −3 of WT-CfMan26A-50K. In the CjMan26A-Glu320Gly−$M_2$ complex, NE of Arg361 forms a hydrogen bond to the C2 hydroxyl of the mannosyl unit at subsite −2 with a length of 2.8 Å, while the NH2 group forms a hydrogen bond with the C3 hydroxyl with a length of 2.9 Å (Figure 1) (*15*, *16*). Although the conformation of Arg323 is different in DM-CfMan26A-50K, interactions with C2 and C3 hydroxyls are plausible in light of the CjMan26A-Glu320Gly−$M_2$ complex. When the two structures are superimposed, Arg323 (DM-CfMan26A-50K) has its NH1 group 3.0 Å from the C3 hydroxyl of the −2 mannosyl unit in the CjMan26A-Glu320Gly−$M_2$ complex and 3.0 Å from the C2 hydroxyl of the same sugar (Figure 1). Hence, the structural data

Scheme 2: Demonstration of Endo-$\beta$-1,4-mannanase-Catalyzed $^{18}O$ Incorporation from $H_2{}^{18}O$ into the Newly Generated Reducing Ends of the Initial Hydrolysis Products of $M_4$[a]

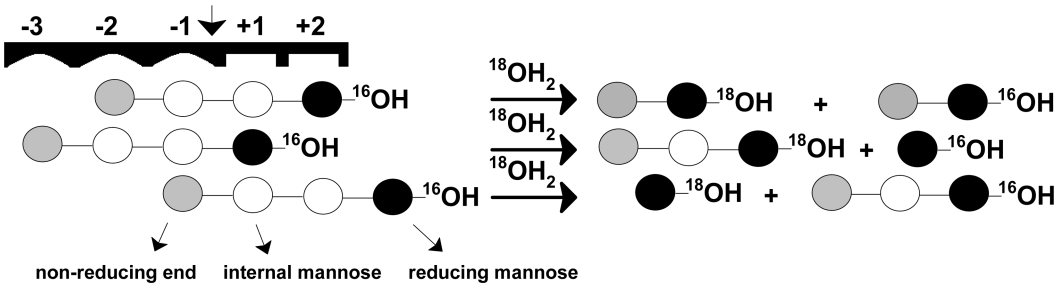


[a]Three parallel reactions resulting from three different productive binding modes are shown.

suggest that the position of a manno-oligosaccharide substrate bound to DM-CfMan26A-50K would be more similar to the one seen for CjMan26A than that for WT-CfMan26A-50K.

*Productive Binding Modes of $M_3$−$M_6$ Analyzed by Isotope Labeling/MS and HPAEC-PAD.* (*i*) *Description of the Methodology*. To determine, in an accurate quantitative manner, how the engineering of subsites −2 and −3 has altered the subsite affinity distribution of the WT enzyme, the WT and DM enzymes have to be compared in terms of their steady-state kinetic parameters as well as the productive binding modes of manno-oligosaccharide substrates. The productive binding modes can be deciphered from a detailed analysis of the initial hydrolytic cleavage patterns of $M_3$−$M_6$ substrates catalyzed by both enzymes. Previous initial-product and kinetic analyses of the WT enzyme gave at hand cleavage patterns of manno-oligosaccharides up to $M_4$ and highlighted the importance of subsite −3 that, judging from the structural data, was potentially contributed by the currently substituted Phe325 (*16*, *24*). In this study, we conducted detailed kinetic and quantitative initial-product analyses of the DM enzyme by HPAEC-PAD and a detailed study of the initial hydrolytic cleavage patterns of $M_3$−$M_6$ catalyzed by both WT and DM enzymes through MALDI-TOF mass spectrometric analysis of $^{18}O$-labeled products (solvent isotope incorporation). The latter method is a further development of a novel straightforward method for determining enzymatic oligosaccharide cleavage patterns, previously established by us for cello-oligosaccharide hydrolysis (*37*). Advantages are the fast analysis by MALDI-TOF MS and the fact that the cleavage pattern can be obtained with the native nonlabeled oligosaccharide. Enzymatic hydrolysis in $H_2{}^{18}O$ results in incorporation of the solvent isotope into the newly generated reducing ends of initial products, in the absence of any detectable nonenzymatic incorporation. During each hydrolytic cleavage reaction, water participation ensures incorporation of $^{18}O$ hydroxyl at the anomeric center (C1) of the mannosyl unit at subsite −1 (Scheme 2). This is in analogy with protease-catalyzed $^{18}O$ incorporation in the newly generated C-termini of peptides utilized in mechanistic studies (*38*, *39*) and proteomics (*40*−*42*). However, only few reports describe glycosidase-catalyzed $^{18}O$ solvent isotope incorporation, including its utilization for carbohydrate structural analysis (*43*), glycosidase activity identification (*44*, *45*), and determination of hydrolytic cleavage patterns of cello- and malto-oligosaccharide substrates (*37*, *46*).

For each substrate oligosaccharide, the relative dominance (frequency) of productive binding modes that give different-DP products can be deduced from initial-product ratios determined by HPAEC-PAD and the relative dominance of each of the two productive binding modes that give the same-DP products can be deduced from MALDI-TOF MS of $^{18}O$-labeled products. For example, one productive binding mode of $M_4$ produces $M_2$ as the only initial product, while two different binding modes both give rise to $M_3$ and $M_1$ (Scheme 2). The frequency of the productive binding mode that gives $M_2$ relative to the other two modes can be determined from the HPAEC-PAD analysis, whereas the relative frequencies of the two modes that both produce $M_3$ and $M_1$ can be determined via MALDI-TOF MS of $^{18}O$-labeled products.

(*ii*) *Comparison of Binding at Subsites −2 and −3*. Using $^{18}O$ labeling and MALDI-TOF MS, we have shown that the predominant productive mode of binding of $M_3$ to the WT enzyme (subsites −2 to +1) has remained the same with the DM enzyme (Figures 3 and 4), consistent with improved subsite −2 binding. On the other hand, MALDI-TOF MS and HPAEC-PAD data reveal that the distal glycone subsite engineering of WT-CfMan26A-50K has a dramatic effect on the initial hydrolysis pattern of $M_4$ making $M_2$ the dominant initial product (instead of $M_3$ and $M_1$ as for the WT enzyme), indicating that the productive binding mode in which $M_4$ occupies subsites −2 to +2 has become predominant (Figures 3−5 and Table 2). This productive binding mode is indeed the major mode of binding of $M_4$ to CjMan26A (*13*), so the action pattern of DM-CfMan26A-50K is more similar to that of CjMan26A. This observation along with the essentially unaffected steady-state kinetic parameters of $M_4$ (Table 3) provides strong evidence of reduced substrate binding at subsite −3 and improved binding at subsite −2 (see the discussion of the steady-state kinetic parameters below). This is also supported by the structural data showing Arg323 of the DM enzyme being suitably positioned for hydrogen bonding to C2 and C3 hydroxyls of mannosyl at subsite −2 (Figures 1 and 2).

The changes in the frequencies of the productive binding modes of larger substrates ($M_5$ and $M_6$) are also consistent with stronger binding at subsite −2 and weaker binding at subsite −3 of the DM enzyme relative to the WT enzyme. The major productive binding mode for $M_5$ has changed from one in which $M_5$ occupies subsites −3 to +2 (in the WT enzyme) to one in which $M_5$ spans subsites −2 to +3 (in the DM enzyme) (Figures 3 and 4). The productive binding modes of $M_6$ in which the nonreducing end of the substrate is bound at subsite −2 have undergone more than 4-fold increases in frequency (Figures 3 and 4).

(*iii*) *Subsite −4*. Curiously, in the case of both $M_5$ and $M_6$ substrates, productive binding modes that exist with the WT enzyme in which subsite −4 is occupied are either greatly weakened or not detected at all with the DM enzyme (Table 2 and Figures 3 and 4). The Phe325 aromatic ring provides stacking interaction at subite −3 of the WT enzyme (*16*) but is far (5−6 Å)

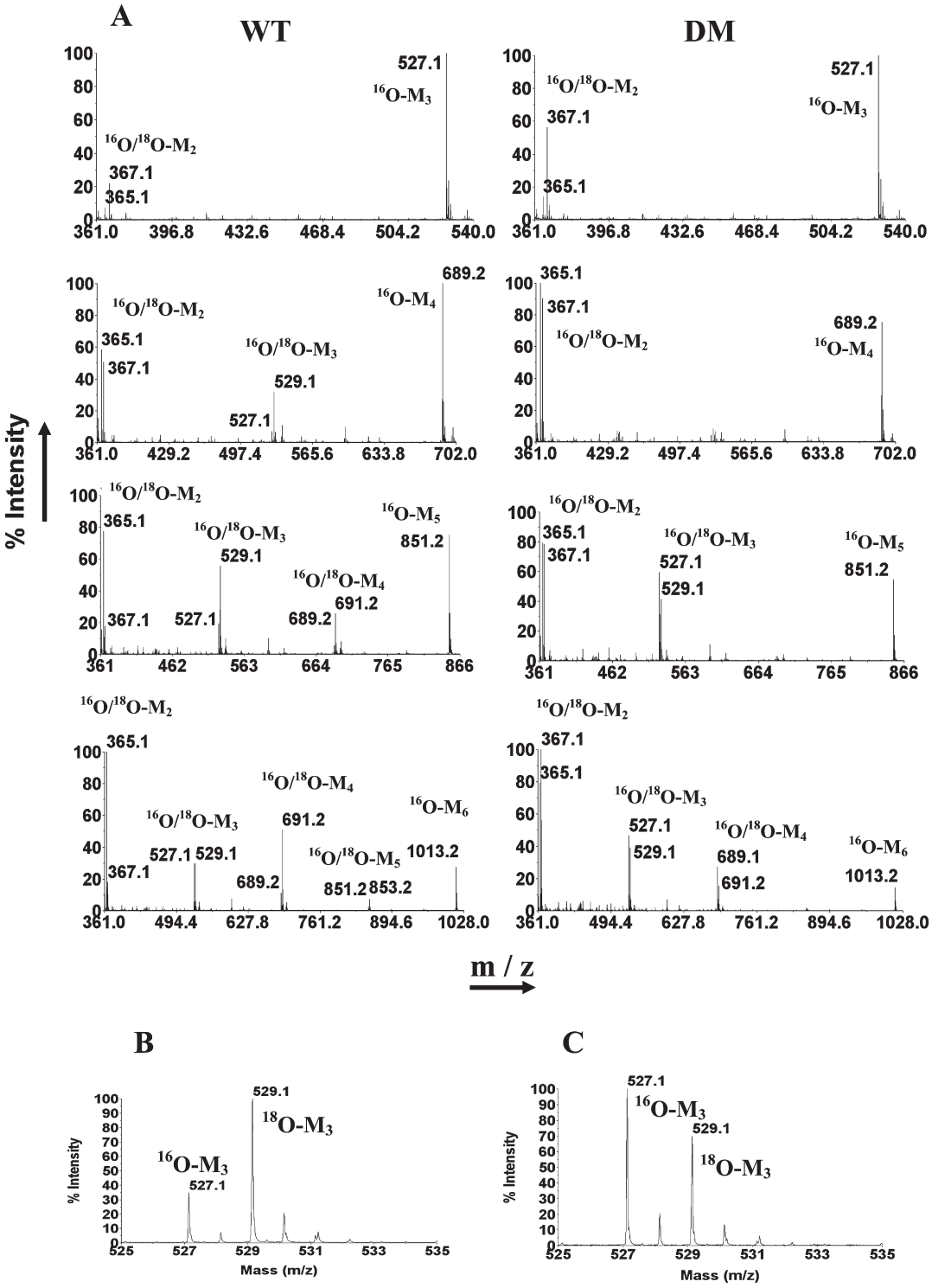


FIGURE 3: MALDI-TOF spectra of hydrolysis products. (A) The initial hydrolytic cleavage patterns of $M_3-M_6$ catalyzed by WT-CfMan26A-50K (left) and DM-CfMan26A-50K (right). Each MALDI-TOF spectrum shows the substrate (from top to bottom, $M_3$, $M_4$, $M_5$, and $M_6$) and the initial products. The $M_1$ product is not detectable because of matrix suppression in the low-mass range (and was quantified by HPAEC-PAD). All peaks represent $[M + Na]^+$ species. Hydrolysis was performed in 93% $H_2{}^{18}O$. During each mannosidic bond cleavage, an $^{18}O$ atom is incorporated at the anomeric center of the newly generated reducing end of one of the products. Each pair of monoisotopic peaks ($\Delta$mass = 2 Da) represents an initial product with either an $^{16}O$ or an $^{18}O$ at the anomeric center of the reducing end, with relative MS peak areas depending on the relative frequencies of the two productive binding modes of the substrate. (B) Enlarged part of the spectrum shown in panel A, where mannopentaose was incubated with the WT enzyme in $H_2{}^{18}O$ showing the hydrolysis products [$^{16}$O]mannotriose and [$^{18}$O]mannotriose with monoisotopic ions at $m/z$ 527.1 and 529.1, respectively. (C) Same as panel B but for the DM enzyme. See the text for details.

from the mannosyl unit at subsite −4 (Figure 1) and loses only ~5 Å$^2$ of accessible surface area when this mannosyl is bound and thus cannot directly contribute to binding at this subsite. Therefore, it appears that some cooperativity (*47*) exists between subsites −3 and −4 in the WT enzyme that has been disrupted and/or weakened by the removal of Phe325 at subsite −3 of the DM enzyme.

In addition, the charged guanidinium side chain of Arg323 might point toward the hydrophobic face of the sugar unit at subsite −3 (Figure 1) and repel it, causing a change in its position

relative to the one in the $M_3$ complex with the WT enzyme. If the mannose unit at subsite −3 of DM-CfMan26A-50K (or CjMan26A) were to sit approximately where it sits in WT-CfMan26A-50K, a steric clash would result, with a distance between the NH2 group of Arg323 and C5 of the mannosyl unit at subsite −3 of only 1.9 Å (Figure 1). Therefore, Arg323 in the DM enzyme (or Arg361 in CjMan26A) seems to play dual roles in substrate binding, making positive mannosyl-binding contributions at subsite −2 but affecting the substrate position at subsite −3 and beyond. Thus, it seems plausible that, with larger substrates $M_5$ and $M_6$, a cooperative effect (*47*) between subsites −3 and −4 in the WT enzyme would result in stronger binding interactions at subsite −4 compared to those in the DM enzyme. There is precedence in the glycosidase literature for the dual roles of nonconserved Arg (*48*). In this case, an Arg provides substrate hydrogen bonding and causes steric hindrance, respectively, in two adjacent subsites.

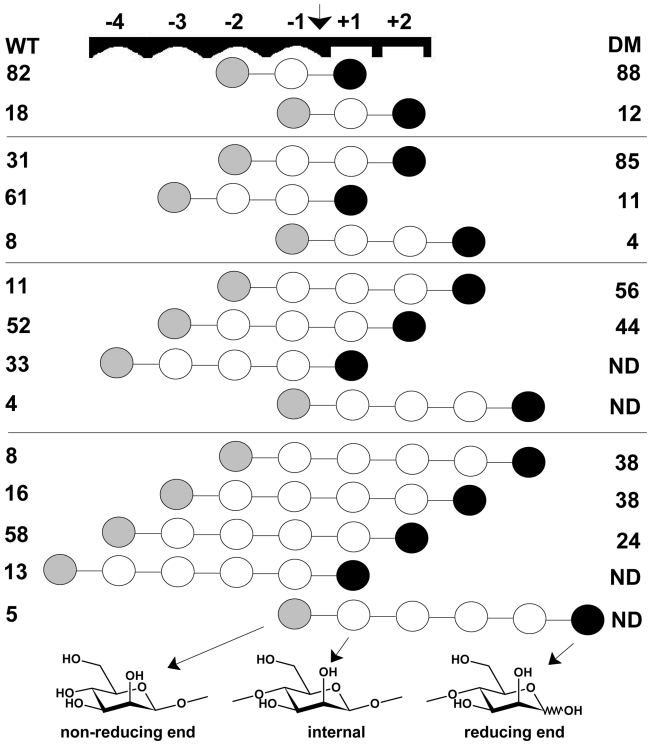


FIGURE 4: Relative dominance (percent) of the productive modes of binding of $M_3$−$M_6$ to WT- and DM-CfMan26A-50K. These were deduced from a quantitative initial-product analysis using HPAEC-PAD (Figure 5 and Table 2) and a detailed analysis of the initial hydrolytic cleavage patterns of $M_3$−$M_6$ using MALDI-TOF MS analysis of $^{18}$O-labeled products (Scheme 2 and Figure 3). The arrow points to the mannosidic bond to be cleaved. See the text for details (ND, not detected).

(*iv*) *Aglycone Binding Subsites*. Our previous kinetic analysis of WT-CfMan26A-50K using $^1$H NMR (*24*) suggested substrate binding involving Trp180 which contributes to binding at subsite +1 and presumably subsite +2 (Figure 1) (*16*). Our current analysis of the DM enzyme also supports the possibility that there is a functional subsite +2 but no binding beyond subsite +2 in the distal aglycone binding region. The relative frequency of the mode of binding of $M_4$ that spans subsites −2 to +2 is almost 8-fold higher than the one that spans subsites −3 to +1 in the DM enzyme (Figure 4). Since both binding modes occupy subsite −2 and binding at subsite −3 has been weakened due to removal of Phe325, this 8-fold effect is at least in part due to the binding contribution of subsite +2. The relative frequency of the mode of binding of $M_5$ that spans subsites −2 to +3 is almost equal to the one that spans subsites −3 to +2 (Figure 4), and similarly, the mode of binding of $M_6$ that spans subsites −2 to +4 has a relative frequency equal to the one that spans subsites −3 to +3, indicating no binding contributions by subsite +3 or +4. There are also no obvious residues that could contribute to substrate binding within subsite +3 or +4.

*Initial and End-Product Ratios Analyzed by HPAEC-PAD. Initial Products of $M_3$−$M_6$ Incubations*. Unlike

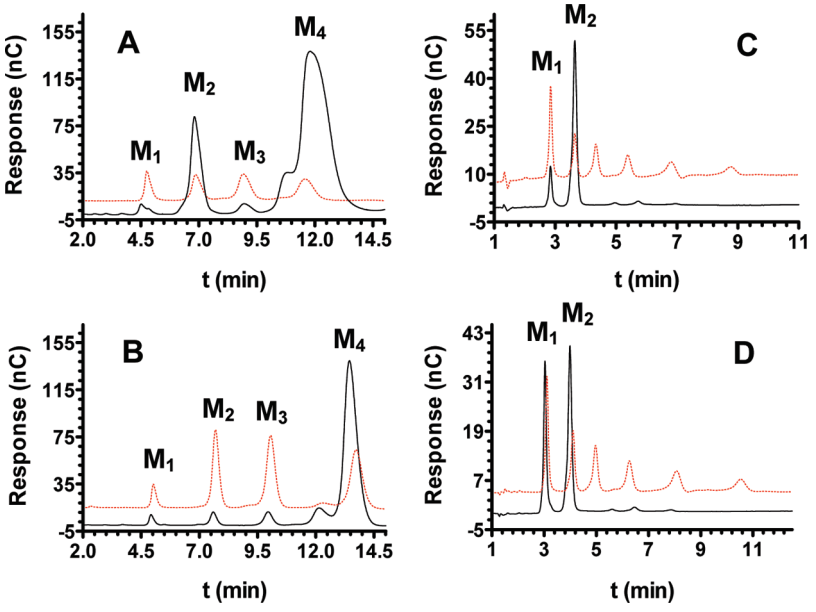


FIGURE 5: Initial and end products of the $M_4$ substrate incubated with WT- and DM-CfMan26A-50K. Each chromatogram shows the analysis using HPAEC-PAD. The solid trace is the chromatogram of a sample of initial or end products, and the dashed trace is the chromatogram of a standard manno-oligosaccharide mixture. See Table 2 for quantitative data and the text for details. (A) Initial products of $M_4$ incubated with DM-CfMan26A-50K. (B) Initial products of $M_4$ incubated with WT-CfMan26A-50K. (C) End products of $M_4$ incubated with DM-CfMan26A-50K. (D) End products of $M_4$ incubated with WT-CfMan26A-50K.

Table 2: Initial and End Products of Manno-Oligosaccharides $M_3-M_6$ Incubated with WT- or DM-CfMan26A-50K

| | | initial product (relative concentration)[a] | | | | | product ratio | |
|---|---|---|---|---|---|---|---|---|
| substrate | enzyme | $M_1$ | $M_2$ | $M_3$ | $M_4$ | $M_5$ | initial-product ratio[b] | end-product ratio ($M_2$:$M_1$) |
| $M_3$ | WT[c] | 1.0 (21) | 1.0 | | | | 1.0 | 1.0 |
| | DM | 1.0 (177) | 1.4 | | | | 1.4 | 1.4 |
| $M_4$ | WT | 1.1 | 1.0 (9.0) | 1.1 | | | 1.0 ($M_3$:$M_1$) | 1.5 |
| | DM | 1.0 (64) | 12.8 | 1.2 | | | 1.2 ($M_3$:$M_1$) | 5.4 |
| $M_5$ | WT | 1.0 (14) | 1.8 | 1.6 | 1.0 | | 0.9 ($M_3$:$M_2$), 1.0 ($M_4$:$M_1$) | 1.3 |
| | DM | | 1.0 (116) | 1.3 | | | 1.3 ($M_3$:$M_2$) | 2.1 |
| $M_6$ | WT | 1.6 | 4.6 | 2.3 | 5.2 | 1.0 (5.2) | 1.1 ($M_4$:$M_2$), 0.6 ($M_5$:$M_1$) | 1.3 |
| | DM | | 1.0 (92) | 1.5 | 1.5 | | 1.5 ($M_4$:$M_2$) | 2.6 |
| LBG | WT | | | | | | | 1.9 |
| | DM | | | | | | | 2.7 |

[a]See the text for experimental details, including substrate concentrations. The initial product with the lowest concentration is shown as 1.0. The actual concentrations (micromolar) are shown in parentheses. [b]Ratio of initial products that add up to the original substrate DP. [c]Initial-product ratios for the hydrolysis of $M_3-M_6$ catalyzed by WT-CfMan26A-50K are from ref *16*. Analysis of $M_4$ initial products of hydrolysis catalyzed by WT-CfMan26A-50K was repeated and reproducible.

Table 3: Steady-State Kinetic Parameters of WT- and DM-CfMan26A-50K for the Hydrolysis of Galactomannans, LBG and GG, and Manno-Oligosaccharides $M_3-M_6$

| substrate | enzyme | $k_{cat}$ ($s^{-1}$) | $K_m$ (mM) | $k_{cat}/K_m$ ($s^{-1}$ $mM^{-1}$) |
|---|---|---|---|---|
| $M_3$ | WT[a] | $1.2 \pm 0.1$ | $3.1 \pm 0.7$ | $0.38 \pm 0.09$ |
| | DM | $0.47 \pm 0.07$ | $2.3 \pm 0.6$ | $0.20 \pm 0.06$ |
| $M_4$ | WT | $11.6 \pm 0.6$ | $2.0 \pm 0.2$ | $5.8 \pm 0.7$ |
| | DM | $3.9 \pm 0.6$ | $2.0 \pm 0.4$ | $2.0 \pm 0.5$ |
| $M_5$ | WT | $52 \pm 1$ | $1.13 \pm 0.06$ | $46 \pm 3$ |
| | DM | $18 \pm 4$ | $9 \pm 2$ | $2.0 \pm 0.6$ |
| $M_6$ | WT | $77 \pm 1$ | $0.69 \pm 0.03$ | $112 \pm 5$ |
| | DM | $27 \pm 5$ | $11 \pm 2$ | $2.5 \pm 0.6$ |
| LBG[b] | WT | $137 \pm 32$ | $1.8 \pm 0.7$ | $76 \pm 32$ |
| | DM | – | – | $8 \pm 1$[c] |
| GG[b] | WT | $137 \pm 31$ | $16 \pm 5$ | $9 \pm 3$ |
| | DM | – | – | $0.66 \pm 0.09$[c] |

[a]Kinetic parameters of WT-CfMan26A-50K for the hydrolysis of $M_3-M_6$ substrates are from ref *16*. [b]$K_m$ values in units of grams per liter and $k_{cat}/K_m$ values in units of liters per gram per second for LBG and GG substrates. [c]Individual $k_{cat}$ and $K_m$ values not determined for DM-CfMan26A-50K because of the lack of saturation over the practical substrate concentration range.

many other mannanases, transglycosylation has not been observed for the WT enzyme (*16*). An intuitive basis has been put forward as indirect evidence of transglycosylation: if transglycosylation occurs on the way to the initial products of oligosaccharide hydrolysis, then the initial products that add up to the original DP of the substrate are produced in nonequimolar quantities; e.g., for $M_4$ hydrolysis, the $M_3$:$M_1$ initial product ratio would not be 1.0, as demonstrated, for example, for GH5 mannanases (*12*). For the WT enzyme, the initial products that add up to the original DP of the substrate are produced in equimolar quantities (Table 2), indicating the absence of native transglycosylation (*16*). However, the initial product ratios are slightly higher than 1.0 for the DM enzyme (Table 2), indicative of weak transglycosylation activity.

*End Products of LBG and $M_3-M_6$ Incubations*. Both WT and DM *C. fimi* enzymes produce $M_2$ and $M_1$ as end products, in contrast to at least some family GH5 mannanases that predominantly produce $M_3$ and $M_2$ (*27*, *49*). The $M_2$:$M_1$ end-product ratios of all substrates are higher for the DM enzyme than for the WT enzyme (Table 2 and Figure 5). This is a logical consequence of the altered initial hydrolytic cleavage patterns that stem from a change in the subsite affinity distribution of the WT enzyme caused by the substitutions. The increase in the $M_2$:$M_1$ ratio is most pronounced for the $M_4$ substrate (4-fold increase compared to that of WT) (Table 2 and Figure 5), which obviously is due to the fact that the predominant initial product of $M_4$ hydrolysis catalyzed by the DM enzyme is $M_2$ (Table 2 and Figure 5). The $M_2$:$M_1$ ratio of 5.4 is similar to a ratio of 4.0 reported for CjMan26A (*50*).

*Steady-State Kinetic Parameters of DM-CfMan26A-50K for the Hydrolysis of $M_3-M_6$ and Polymers*. Notably, the observed $k_{cat}$ value of the DM enzyme for each respective oligomeric substrate is only ~3-fold lower than that of the WT enzyme (Table 3), and the observed $k_{cat}$ values of both enzymes follow the same pattern of increasing from $M_3$ to $M_6$. Assuming that the observed $k_{cat}$ values represent the intrinsic rate constants for a chemical step, the fact that they are within the same order of magnitude for both enzymes suggests that the positions of key catalytic residues and the proximity and orientation of the glycosidic bond to be cleaved have not been disturbed to any significant extent as a consequence of the mutations (*51*). Indeed, the rmsd for the catalytic residues and residues within 5 Å of subsites −1 to −4 of WT-CfMan26A-50K and DM-CfMan26A-50K is only 0.32 Å for all atoms.

Remarkably, the observed $K_m$ values of the DM enzyme for $M_3$ and $M_4$ substrates are identical to those of the WT enzyme within experimental error (Table 3); hence, the observed $k_{cat}/K_m$ values are within the same order of magnitude. In the case of the $M_4$ substrate, this provides the strongest evidence of the improvement of the subsite −2 affinity and the decline of the subsite −3 affinity by the mutations (assuming $K_m$ approximates $K_s$). If the substrate binding affinity of subsite −2 had not improved upon the introduction of Arg323 and the productive binding mode involving subsites −2 to +2 had been favored over the one involving subsites −3 to +1 (Figure 4) simply because the binding affinity of subsite −3 had declined (removal of Phe325), then the overall apparent affinity of the DM enzyme for $M_4$ would have decreased, i.e., higher observed $K_m$ value relative to that of the WT enzyme.

The major productive modes of binding of $M_3$ to both enzymes are the same (−2 to +1). The explanation for why the observed $K_m$ value of the DM enzyme for $M_3$ is almost the same as that of the WT enzyme is as follows: it is clear from the hyperbolic steady-state initial rate equation for a multisubsite enzyme (*51*−*54*) that

the observed $k_{cat}$ and $K_m$ values include both productive and nonproductive binding terms for the oligomeric substrate, whereas the observed $k_{cat}/K_m$ value includes only the productive binding terms. In the case of the WT enzyme, at least one nonproductive binding mode has been observed in the crystal structure (*16*) in which $M_3$ binds from subsites −4 to −2. This nonproductive mode likely contributes to the lowering of the observed $K_m$ value of the WT enzyme for $M_3$, making it almost equal to the observed $K_m$ for $M_4$ (Table 3), but it has most likely been disrupted or weakened in the DM enzyme because of the decline of the affinities of both subsites −4 and −3. In fact, all attempts to determine a structure of the DM enzyme in a nonproductive complex with $M_3$ through soaking experiments in a manner similar to that for the WT enzyme failed.

Similar to many other polysaccharidases, the WT enzyme has decreasing $K_m$ values with increasing substrate DP's. Interestingly, the observed $K_m$ values of the DM enzyme for $M_5$ and $M_6$ are higher than those for $M_3$ and $M_4$ and also higher than those of the WT enzyme for $M_3$−$M_6$ (Table 3). Given that the WT or DM enzymes do not utilize significant binding contributions by the distal aglycone subsites, the contributions of distal glycone subites −3 and beyond are more crucial for optimal binding of these larger substrates $M_5$ and $M_6$ than of $M_3$ and $M_4$, as one can see from their productive binding modes (Figure 4). In the DM enzyme, the lack of Phe325 weakens substrate binding at subsite −3, and in addition, the steric clash with the side chain of Arg323 at subsite −3 must cause spatial repositioning of mannosyl units of the substrate occupying subsites −3 and beyond away from the binding groove (as discussed above in Subsite −4). In fact, this phenomenon is even more pronounced with the polymeric LBG and GG substrates where no saturation was observed over the practical concentration ranges, because of the poorer binding of these substrates to the DM enzyme, and only the observed $k_{cat}/K_m$ values could be determined (Table 3). Similarly, the two GH26 *Ce. japonicus* enzymes, CjMan26A and -C, which have a high-affinity Arg at their −2 subsites but lack a Phe at their −3 subsites exhibit unusually high activity against small manno-oligosaccharides $M_3$ and $M_4$ compared to polysaccharides (*19*).

*General Discussion*. Using the *C. fimi* β-mannanase as an example, we have demonstrated protein engineering of nonconserved glycone-binding subsites (−3 and −2) of GH26 enzymes. Phe325 of subsite −3 was substituted with Ala, leaving room for the Ala323Arg substitution which introduced an Arg in a position equivalent to that in the homologous β-mannanase, CjMan26A, where it interacts specifically and with high affinity with mannosyl at subsite −2. 3D structure determination of the DM enzyme confirmed successfully that the Arg is in a position similar, although not identical, to that in the template enzyme (CjMan26A) (Figures 1 and 2). The application of a facile method to analyze relative subsite affinities involving enzymatic assays in $^{18}O$ water and MS analysis (Scheme 2 and Figures 3 and 4) provided valuable information together with HPAEC-PAD analysis (Figure 5 and Table 2). These analyses successfully demonstrated that the DM enzyme has an altered hydrolytic cleavage pattern that stems from the promotion of mannosyl affinity in subsite −2 and demotion of it in subsite −3 (mimicking CjMan26A). This is most clearly seen for the $M_4$ substrate having a productive complex predominantly binding with the nonreducing mannosyl at subsite −3 for the WT enzyme but at subsite −2 for the DM enzyme (Figure 4), while the observed $K_m$ value is unaffected (Table 3).

Site-directed mutagenesis of subsites within polysaccharidases has been widely reported. Not surprisingly, substitutions of amino acid residues involved in binding and/or catalysis at the crucial proximal −1 glycone subsite, at which the sugar ring undergoes conformational changes (*19*, *21*), to residues that lack the required functionalities (e.g., Ala and Gly) usually have severe effects on the activity against both oligo- and polysaccharides alike (*13*, *55*, *56*). However, a pattern seems to have emerged for the glycosidase variants with single substitutions in either distal glycone (mainly −2) or proximal/distal aglycone subsites (mainly +1) in which the substitutions seem to have a greater negative influence on the activity of glycosidase against oligosaccharide than polysaccharide substrates. Examples are altered subsites −2 and +1 of CjMan26A (*13*, *19*) and subsite −2 variants of a *Ce. japonicus* GH10 xylanase (*55*, *57*, *58*). In this light, our DM enzyme appears exceptional since the activity toward polymeric substrate suffers but the activity on oligomers up to $M_4$ is in essence unaffacted. This is because rather than simply removing a residue important for binding in a single subsite (in our case Phe325 in subsite −3) we have also introduced a substrate binding residue in an adjacent subsite (Arg323 in subsite −2) that compensates for the loss of affinity. Consequently, the DM enzyme has nativelike catalytic activity ($k_{cat}/K_m$) against smaller manno-oligosaccharides $M_3$ and $M_4$ (Table 3). However, the activity against larger manno-oligosaccharides and polysaccharids has suffered by 1 order of magnitude, possibly due to Arg323, causing substrate repulsion at subsite −3 and likely affecting also subsites −4 and beyond, as discussed in previous sections.

*Concluding Remarks*. This work demonstrates that, in general, subsite structure of glycanases can be rationally redesigned via not only removal of functionalities essential for substrate binding but also introduction of such functionalities (*59*) on the basis of structural and functional analogies. In particular, amino acid residues such as Arg that specifically interact with axial C2 hydroxyl could be engineered into one of the subsites (except subsite −1) of a β-mannanase to improve mannose binding. However, intricate structural roles of introduced residues, e.g., the dual role of Arg323 in the engineered DM enzyme, may lead to subtle and unexpected functional consequences such as the observed lower activity against polymeric substrates. Finally, the design of the doubly substituted enzyme variant could be used as a starting point for further rational and random optimization toward higher transglycosylating capacity. A β-mannan synthase with better binding at subsite −2 could indeed bind synthetic donor substrate α-mannobiosyl fluoride more tightly (*15*) for more efficient synthesis.

## ACKNOWLEDGMENT

We thank Jonatan Göth for performing mutagenesis, Wietske Lambert for help with mass spectrometry, and Herje Schagerlöf for useful discussions (all at Lund University). We also thank Dorthe Boelskifte and Jens-Christian Navarro Poulsen for assistance with the crystallization robot at the University of Copenhagen. MAXLAB is acknowledged for beam time.

## REFERENCES

1. Lundqvist, J., Teleman, A., Junel, L., Zaachi, G., Dahlman, O., Tjerneld, F., and Stalbrand, H. (2002) Isolation and characterization of galactoglucomannan from Spruce (*Picea abies*). *Carbohydr. Polym.* *48*, 29–39.

2. Gilbert, H. J., Stalbrand, H., and Brumer, H. (2008) How the walls come crumbling down: Recent structural biochemistry of plant polysaccharide degradation. *Curr. Opin. Plant Biol. 11*, 338–348.
3. Cantarel, B. L., Coutinho, P. M., Rancurel, C., Bernard, T., Lombard, V., and Henrissat, B. (2009) The Carbohydrate-Active EnZymes database (CAZy): An expert resource for Glycogenomics. *Nucleic Acids Res. 37*, D233–D238.
4. Jenkins, J., Lo Leggio, L., Harris, G., and Pickersgill, R. (1995) $\beta$-Glucosidase, $\beta$-galactosidase, family A cellulases, family F xylanases and two barley glucanases form a superfamily of enzymes with 8-fold $\beta/\alpha$ architecture and with two conserved glutamates near the carboxy-terminal ends of $\beta$-strands four and seven. *FEBS Lett. 362*, 281–285.
5. Henrissat, B., Callebaut, I., Fabrega, S., Lehn, P., Mornon, J.-P., and Davies, G. (1995) Conserved catalytic machinery and the prediction of a common fold for several families of glycosyl hydrolases. *Proc. Natl. Acad. Sci. U.S.A. 92*, 7090–7094.
6. Zechel, D. L., and Withers, S. G. (2000) Glycosidase mechanisms: Anatomy of a finely tuned catalyst. *Acc. Chem. Res. 33*, 11–18.
7. Hägglund, P., Eriksson, T., Collen, A., Nerinckx, W., Claeyssen, M., and Stalbrand, H. (2003) A cellulose binding module of a *Trichoderma reesei* $\beta$-1,4-mannanase increases the mannan-hydrolysis of complex. *J. Biotechnol. 101*, 37–48.
8. Boraston, A. B., Bolam, D. N., Gilbert, H. J., and Davies, G. J. (2004) Carbohydrate-binding modules: Fine-tuning polysaccharide recognition. *Biochem. J. 382*, 769–781.
9. Hilge, M., Gloor, S. M., Rypniewski, W., Sauer, O., Heightman, T. D., Zimmermann, W., Winterhalter, K., and Piontek, K. (1998) High-resolution native and complex structures of thermostable $\beta$-mannanase from *Thermomonospora fusca*-substrate specificity in glycosyl hydrolase family 5. *Structure 6*, 1433–1444.
10. Sabini, E., Schubert, H., Murshudov, G., Wilson, K. S., Siika-Aho, M., and Penttilä, M. (2000) The three-dimensional structure of a *Trichoderma reesei* $\beta$-mannanase from glycoside hydrolase family 5. *Acta Crystallogr. D56*, 3–13.
11. Bourgault, R., Oakley, A. J., Bewley, J. D., and Wilce, M. C. (2005) Three-dimensional structure of (1,4)-$\beta$-D-mannan mannanohydrolase from tomato fruit. *Protein Sci. 14*, 1233–1241.
12. Larsson, A. M., Anderson, L., Xu, B., Muñoz, I. G., Usón, I., Janson, J. C., Stalbrand, H., and Stahlberg, J. (2006) Three-dimensional crystal structure and enzymic characterization of $\beta$-mannanase Man5A from blue mussel *Mytilus edulis*. *J. Mol. Biol. 357*, 1500–1510.
13. Hogg, D., Woo, E. J., Bolam, D. N., McKie, V. A., Gilbert, H. J., and Pickersgill, R. W. (2001) Crystal structure of mannanase 26A from *Pseudomonas cellulosa* and analysis of residues involved in substrate binding. *J. Biol. Chem. 276*, 31186–31192.
14. Ducros, V. M., Zechel, D. L., Murshudov, G. N., Gilbert, H. J., Szabo, L., Stoll, D., Withers, S. G., and Davies, G. J. (2002) Substrate distortion by a $\beta$-mannanase: Snapshots of the Michaelis and covalent-intermediate complexes suggest a $B_{(2,5)}$ conformation for the transition state. *Angew. Chem., Int. Ed. 41*, 2824–2827.
15. Jahn, M., Stoll, D., Warren, R. A., Szabó, L., Singh, P., Gilbert, H. J., Ducros, V. M., Davies, G. J., and Withers, S. G. (2003) Expansion of the glycosynthase repertoire to produce defined manno-oligosaccharides. *Chem. Commun. 12*, 1327–1329.
16. Le Nours, J., Anderson, L., Stoll, D., Stalbrand, H., and Lo Leggio, L. (2005) The structure and characterization of a modular endo-$\beta$-1,4-mannanase from *Cellulomonas fimi*. *Biochemistry 44*, 12700–12708.
17. Cartmell, A., Topakas, E., Ducros, V. M., Suits, M. D., Davies, G. J., and Gilbert, H. J. (2008) The *Cellvibrio japonicus* mannanase CjMan26C displays a unique exo-mode of action that is conferred by subtle changes to the distal region of the active site. *J. Biol. Chem. 283*, 34403–34413.
18. Yan, X. X., An, X. M., Gui, L. L., and Liang, D. C. (2008) From structure to function: Insights into the catalytic substrate specificity and thermostability displayed by *Bacillus subtilis* mannanase BCman. *J. Mol. Biol. 379*, 535–544.
19. Tailford, L. E., Ducros, V. M., Flint, J. E., Roberts, S. M., Morland, C., Zechel, D. L., Smith, N., Bjornvad, M. E., Borchert, T. V., Wilson, K. S., Davies, G. J., and Gilbert, H. J. (2009) Understanding how diverse $\beta$-mannanases recognize heterogeneous substrates. *Biochemistry 48*, 7009–7018.
20. Davies, G. J., Wilson, K. S., and Henrissat, B. (1997) Nomenclature for sugar-binding subsites in glycosyl hydrolases. *Biochem. J. 321*, 557–559.
21. Tailford, L. E., Offen, W. A., Smith, N. L., Dumon, C., Morland, C., Gratien, J., Heck, M. P., Stick, R. V., Bleriot, Y., Vasella, A., Gilbert, H. J., and Davies, G. J. (2008) Structural and biochemical evidence for a boat-like transition state in $\beta$-mannosidases. *Nat. Chem. Biol. 4*, 306–312.
22. Stoll, D., Stalbrand, H., and Warren, R. A. J. (1999) Mannan-degrading enzymes from *Cellulomonas fimi*. *Appl. Environ. Microbiol. 65*, 2598–2605.
23. Stoll, D., Boraston, A., Stalbrand, H., McLean, B. W., Kilburn, D. G., and Warren, R. A. J. (2000) Mannanase Man26A from *Cellulomonas fimi* has a mannan-binding module. *FEMS Microbiol. Lett. 183*, 265–269.
24. Anderson, L., Hägglund, P., Stoll, D., Lo Leggio, L., Drakenberg, T., and Stalbrand, H. (2008) Kinetics and stereochemistry of the *Cellulomonas fimi* $\beta$-mannanase studied using $^1$H-NMR. *Biocatal. Biotransform. 26*, 86–95.
25. Bolam, D. N., Hughes, N., Virden, R., Lakey, J. H., Hazlewood, G. P., Henrissat, B., Braithwaite, K. L., and Gilbert, H. J. (1996) Mannanase A from *Pseudomonas fluorescens ssp. cellulosa* is a retaining glycosyl hydrolase in which E212 and E320 are the putative catalytic residues. *Biochemistry 35*, 16195–16204.
26. Horton, R. M., Hunt, H. D., Ho, S. N., Pullen, J. K., and Pease, L. R. (1989) Site-directed mutagenesis by overlap extension using the polymerase chain reaction. *Gene 77*, 61–68.
27. Stalbrand, H., Siika-aho, M., Tenkanen, M., and Viikari, L. (1993) Purification and characterization of two $\beta$-mannanases from *Trichoderma reesei*. *J. Biotechnol. 29*, 229–242.
28. Leslie, A. G. (1999) Integration of macromolecular diffraction data. *Acta Crystallogr. D55*, 1696–1702.
29. Evans, P. R. (1997) Scaling of MAD data. *Joint CCP4 and ESF-EACBM Newsletter 33*, 22–24.
30. Weiss, M. S. (2001) Global indicators of X-ray data quality. *J. Appl. Crystallogr. 34*, 130–135.
31. Laskowski, R. A., MacArthur, M. W., Moss, D. S., and Thornton, J. M. (1993) PROCHECK: A program to check the stereochemical quality of protein structures. *J. Appl. Crystallogr. 26*, 283–291.
32. Vagin, A., and Teplyakov, A. (1997) MOLREP: An automated program for molecular replacement. *J. Appl. Crystallogr. 30*, 1022–1025.
33. Murshudov, G. N., Vagin, A. A., and Dodson, E. J. (1997) Refinement of macromolecular structures by the maximum-likelihood method. *Acta Crystallogr. D53*, 240–255.
34. Emsley, P., and Cowtan, K. (2004) Coot: Model-building tools for molecular graphics. *Acta Crystallogr. D60*, 2126–2132.
35. Perrakis, A., Morris, R. M., and Lamzin, V. S. (1999) Automated protein model building combined with iterative structure refinement. *Nat. Struct. Biol. 6*, 458–463.
36. Bounias, M. (1980) N-(1-naphthyl)ethylenediamine dihydrochloride as a new reagent for nanomole quantification of sugars on thin-layer plates by a mathematical calibration process. *Anal. Biochem. 106*, 291–295.
37. Schagerlöf, H., Nilsson, C., Gorton, L., Tjerneld, F., Stalbrand, H., and Cohen, A. (2009) Use of $^{18}$O water and ESI-MS detection in subsite characterisation and investigation of the hydrolytic action of an endoglucanase. *Anal. Bioanal. Chem. 394*, 1977–1984.
38. Antonov, V. K., Ginodman, L. M., Rumsh, L. D., Kapitannikov, Y. V., Barshevskaya, T. N., Yavashev, L. P., Gurova, A. G., and Volkova, L. I. (1981) Studies on the mechanisms of action of proteolytic enzymes using heavy oxygen exchange. *Eur. J. Biochem. 117*, 195–200.
39. Angeles, T. S., Roberts, G. A., Carr, S. A., and Meek, T. D. (1992) Solvent isotope partitioning: A new kinetic tool for the determination of desorption rates of reactant water from enzyme-substrate complexes in proteases. *Biochemistry 31*, 11778–11784.
40. Julka, S., and Regnier, F. (2004) Quantification in proteomics through stable isotope coding: A review. *J. Proteome Res. 3*, 350–363.
41. Leitner, A., and Lindner, W. (2004) Current chemical tagging strategies for proteome analysis by mass spectrometry. *J. Chromatogr., B 813*, 1–26.
42. Miyagi, M., and Rao, K. C. (2007) Proteolytic $^{18}$O-labeling strategies for quantitative proteomics. *Mass Spectrom. Rev. 26*, 121–136.
43. Tüting, W., Wegemann, K., and Mischnick, P. (2004) Enzymatic degradation and electrospray tandem mass spectrometry as tools for determining the structure of cationic starches prepared by wet and dry methods. *Carbohydr. Res. 339*, 637–648.
44. Varki, A., Sherman, W., and Kornfeld, S. (1983) Demonstration of the enzymatic mechanisms of $\alpha$-N-acetyl-D-glucosamine-1-phosphodiester N-acetylglucosaminidase (formerly called $\alpha$-N-acetylglucosaminylphosphodiesterase) and lysosomal $\alpha$-N-acetylglucosaminidase. *Arch. Biochem. Biophys. 222*, 145–149.
45. Kiso, T., Nakano, H., Nakajima, H., Terai, T., Okamoto, K., and Kitahata, S. (2000) Hydrolysis of $\beta$-galactosyl ester linkage by $\beta$-galactosidases. *Biosci., Biotechnol., Biochem. 64*, 1702–1706.

46. Kato, M., Takehara, K., Kettoku, M., Kobayashi, K., and Shimizu, T. (2000) Subsite structure and catalytic mechanism of a new glycosyltrehalose-producing enzyme isolated from the hyperthermophilic archaeum, *Sulfolobus solfataricus* KM1. *Biosci., Biotechnol., Biochem. 64*, 319–326.
47. Haga, K., Kanai, R., Sakamoto, O., Aoyagi, M., Harata, K., and Yamane, K. (2003) Effects of essential carbohydrate/aromatic stacking interaction with Tyr100 and Phe259 on substrate binding of cyclodextrin glycosyltransferase from alkalophilic *Bacillus* sp. 1011. *J. Biochem. 134*, 881–891.
48. Albenne, C., Skov, L. K., Mirza, O., Gajhede, M., Feller, G., D'Amico, S., André, G., Potocki-Véronèse, G., van der Veen, B. A., Monsan, P., and Remaud-Simeon, M. (2004) Molecular basis of the amylose-like polymer formation catalyzed by *Neisseria polysaccharea* amylosucrase. *J. Biol. Chem. 279*, 726–734.
49. Ademark, P., Varga, A., Medve, J., Harjunpää, V., Drakenberg, T., Tjerneld, F., and Stalbrand, H. (1998) Softwood hemicellulose-degrading enzymes from *Aspergillus niger*: Purification and properties of a $\beta$-mannanase. *J. Biotechnol. 63*, 199–210.
50. Braithwaite, K. L., Black, G. W., Hazlewood, G. P., Ali, B. R., and Gilbert, H. J. (1995) A non-modular endo-$\beta$-1,4-mannanase from *Pseudomonas fluorescens* subspecies *cellulosa*. *Biochem. J. 305*, 1005–1010.
51. Fersht, A. (1999) Structure and Mechanism in Protein Science, W. H. Freeman and Co., New York.
52. Hekmat, O., Tokuyasu, K., and Withers, S. G. (2003) Subsite structure of the endo-type chitin deacetylase from a deuteromycete, *Colletotrichum lindemuthianum*: An investigation using steady-state kinetic analysis and MS. *Biochem. J. 374*, 369–380.
53. Thoma, J. A., Rao, G. V., Brothers, C., Spradlin, J., and Li, L. H. (1971) Subsite mapping of enzymes. Correlation of product patterns with Michaelis parameters and substrate-induced strain. *J. Biol. Chem. 246*, 5621–5635.
54. Allen, J. D. (1980) Subsite mapping on enzymes: Application to polysaccharide depolymerases. *Methods Enzymol. 64*, 248–277.
55. Charnock, S. J., Spurway, T. D., Xie, H., Beylot, M. H., Virden, R., Warren, R. A., Hazlewood, G. P., and Gilbert, H. J. (1998) The topology of the substrate binding clefts of glycosyl hydrolase family 10 xylanases are not conserved. *J. Biol. Chem. 273*, 32187–32199.
56. Ly, H. D., and Withers, S. G. (1999) Mutagenesis of glycosidases. *Annu. Rev. Biochem. 68*, 487–522.
57. Charnock, S. J., Lakey, J. H., Virden, R., Hughes, N., Sinnott, M. L., Hazlewood, G. P., Pickersgill, R., and Gilbert, H. J. (1997) Key residues in subsite F play a critical role in the activity of *Pseudomonas fluorescens* subspecies *cellulosa* xylanase A against xylooligosaccharides but not against highly polymeric substrates such as xylan. *J. Biol. Chem. 272*, 2942–2951.
58. Armand, S., Andrews, S. R., Charnock, S. J., and Gilbert, H. J. (2001) Influence of the aglycone region of the substrate binding cleft of *Pseudomonas* xylanase 10A on catalysis. *Biochemistry 40*, 7404–7409.
59. Bak-Jensen, K. S., Andre, G., Gottschalk, T. E., Paes, G., Tran, V., and Svensson, B. (2004) Tyrosine 105 and threonine 212 at outermost substrate binding subsites $-6$ and $+4$ control substrate specificity, oligosaccharide cleavage patterns, and multiple binding modes of barley $\alpha$-amylase 1. *J. Biol. Chem. 279*, 10093–10102.